6-22-2020

Strain-Enhanced Metallic Intermixing in Shape-Controlled Multilayered Core–Shell Nanostructures: Toward Shaped Intermetallics

Benjamin P. Williams
Boston College

Allison P. Young
Boston College

Ilektra Andoni
Boston College

Yong Han
Iowa State University, y27h@iastate.edu

Wei-Shang Lo
Boston College

See next page for additional authors

Strain-Enhanced Metallic Intermixing in Shape-Controlled Multilayered Core–Shell Nanostructures: Toward Shaped Intermetallics

Abstract

Controlling the surface composition of shaped bimetallic nanoparticles could offer precise tunability of geometric and electronic surface structure for new nanocatalysts. To achieve this goal, a platform for studying the intermixing process in a shaped nanoparticle was designed, using multilayered Pd-Ni-Pt core–shell nanocubes as precursors. Under mild conditions, the intermixing between Ni and Pt could be tuned by changing layer thickness and number, triggering intermixing while preserving nanoparticle shape. Intermixing of the two metals is monitored using transmission electron microscopy. The surface structure evolution is characterized using electrochemical methanol oxidation. DFT calculations suggest that the low-temperature mixing is enhanced by shorter diffusion lengths and strain introduced by the layered structure. The platform and insights presented are an advance toward the realization of shape-controlled multimetallic nanoparticles tailored to each potential application.

Keywords

multilayered core–shell nanostructures, shaped intermetallic nanoparticles, strain-enhanced metallic intermixing

Disciplines

Engineering Physics | Materials Chemistry | Nanoscience and Nanotechnology

Authors

Benjamin P. Williams, Allison P. Young, Ilektra Andoni, Yong Han, Wei-Shang Lo, Matthew Golden, Jane Yang, Lian-Ming Lyu, Chun-Hong Kuo, James W. Evans, Wenyu Huang, and Chia-Kuang Tsung

Strain-Driven Metallic Intermixing in Shape-Controlled Multilayered Core-Shell Nanostructures: Toward Shaped Intermetallics

Benjamin P. Williams[†,‡], Allison P. Young[†,‡], Ilektra Andoni[‡], Yong Han[#], Wei-Shang Lo[‡], Matthew Golden[‡], Jane Yang[‡], Chen-Rui Kao[^], Chun-Hong Kuo[^], James W. Evans[#], Wenyu Huang[§], and Chia-Kuang Tsung*[,‡]

[‡]Department of Chemistry, Merkert Chemistry Center, Boston College, 2609 Beacon Street, Chestnut Hill, Massachusetts 02467, United States.

[#]Ames Laboratory – USDOE and Department of Physics & Astronomy, Iowa State University, Ames, Iowa 50011.

[§]Ames Laboratory – USDOE and Department of Chemistry, Iowa State University, Ames, Iowa 50011.

[^]Institute of Chemistry, Academia Sinica, No. 128, Section 2, Academia Rd, Nangang District, Taipei City, Taiwan 115.

[†]These authors contributed equally to this work.

Supporting Information Placeholder

ABSTRACT: Controlling the surface composition of shaped bimetallic nanoparticles could offer precise tunability of geometric and electronic surface structure for new nanocatalysts. To achieve this goal, we design a platform for studying the intermixing process in a shaped nanoparticle, using multilayered Pd-Ni-Pt core-shell nanocubes as precursors. We find that, under mild conditions, the intermixing between Ni and Pt could be tuned by changing layer thickness and number, triggering intermixing while preserving nanoparticle shape. Intermixing of the two metals is monitored using transmission electron microscopy. The surface structure evolution is characterized using electrochemical methanol oxidation. DFT calculations suggest that the low-temperature mixing is enhanced by strain introduced by the layered structure. The platform and insights presented here represent an advance toward the realization of shape-controlled multimetallic nanoparticles tailored to each potential application.

Nanomaterial design has increasingly focused on developing highly active and stable catalysts for chemical transformations[1-9]. Platinum group metals are particularly active for a diverse set of reactions, but they are expensive and susceptible to surface poisoning. By incorporating nonprecious metals, catalyst cost can be lowered and performance can be improved[10-16]. The degree of intermixing between the metals has recently been shown to dramatically affect catalyst performance, but the mechanism of mixing is not well understood.[2, 17-18] Thus, we aim to study the intermixing process and clarify its effect on catalysis.

Among alloys, the compositions that form intermetallic compounds (IMCs) have attracted recent attention because, in these cases, intermixing is thermodynamically favored. Generally, IMCs are crystalline alloys composed of two or more metallic/metalloid elements with specific stoichiometry and long-range order. More robust and resilient to etching[19], these atomically ordered structures offer unique properties, including shape-memory[20], hydrogen storage[21], and superconductivity[22]. Further, their tunable surface electronic structures[23-25] allow their adsorption and desorption properties to be tailored to specific chemical reactions. In previous works, bulk IMCs have been extensively studied. More recent studies have focused on IMC nanoparticles (NPs) for their tailorable geometries, electronic surface structures and molecular adsorption properties[26-34]. The kinetics of solid-state intermixing to form IMCs, however, has received little attention.

We note three approaches to the formation of IMC NPs[29, 35]. The first is a top-down synthesis method, where particles are formed by the mechanical alloying of mixed metallic powders through ball milling and annealing to form IMC phases[34]. The size and shape of particles synthesized by these methods cannot be controlled, and no information can be gained on the nanoscale intermixing process. The second is direct, bottom-up synthesis by wet-chemistry methods. Shaped IMC NPs have been generated using this method[36-37], but the need to precisely and simultaneously control the deposition rates of the chosen metals makes extending their scope and understanding their formation kinetics challenging. The third reported strategy involves synthesizing alloyed or heterostructured bimetallic NPs (e.g. core-shell or dimer) by wet-chemistry and then converting these NPs to the intermetallic phase through intermixing triggered by thermal annealing at high temperatures[38]. While promising, intermixing under these harsh conditions degrades the NP, generally through sintering and reshaping, preventing the study of intermixing in a specific geometry. The resulting indistinct particle shapes can further convolute catalytic results due to inconsistencies in size, shape/faceting, and surface composition, making the fundamental study of the catalyst surface or active sites difficult. In this work, we aim to optimize this third approach because we believe that intermixing, taking place in well-controlled nanoscale geometries, offers the best opportunity to understand the shape-dependent formation kinetics of IMC phases, which could, in turn, lead to a general synthesis scheme for shaped IMC NPs.

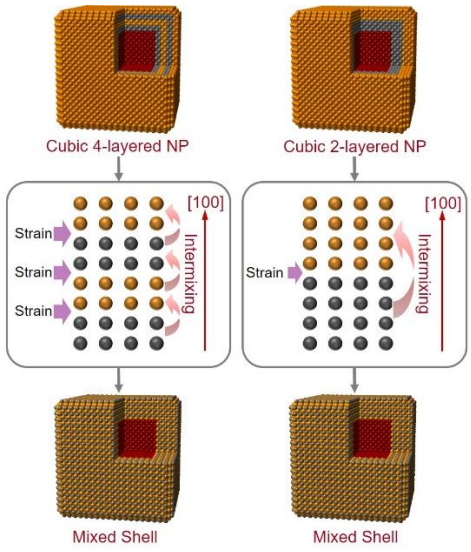

Scheme 1: Schematic representation of the conversion process from shaped Pd-Ni-Pt and Pd-$(Ni-Pt)_2$

nanoparticle precursors to Pd-Ni_3Pt core-mixed shell structures through atomic diffusion.

Since the solid-solid interdiffusion of metal atoms to form ordered intermetallic structures is the greatest contributor to the need for high annealing temperatures [39-41], we focus on lowering the effective diffusion barriers, which we hypothesize can be reduced by the use of strained metallic layers of variable thickness. Moreover, varying the layer thickness could allow us to test the effect of these variables on metallic mixing. Structures with a higher number of thinner layers (and thus higher strain and shorter diffusion lengths), we hypothesize, should show mixing at lower temperature than those with fewer, thicker layers. Previously, our group developed defined overgrowth methods for well-controlled core-shell NPs using mild aqueous phase systems[12-13, 42]. During these syntheses, variables such as substrate size and shape, layer thickness and compositions, and layer number could be controlled. Notably, our Pd-Ni-Pt system[13] stands out as an interesting candidate for the study of intermetallic formation, as the incorporation of Ni into Pt NPs has been shown to increase catalytic activity towards small molecule redox reactions[10-11, 19, 43]. This well-defined platform serves as an ideal arena to study intermetallic formation, because this controlled, layered structure allows for a simple mixing process that can be easily characterized compared to other systems, such as alloy nanoparticles (Scheme 1). Herein, we focus on the $PtNi_3$ system as it has the highest loading of the nonprecious metal, Ni, relative to the precious metal, Pt. To maintain a bimetallic and more easily studied system, the core particle used to direct the shape of the NPs should be inert to the layer above it. For this reason, the Pd core was chosen; Pd and Ni are not known to form stable IMC phases under mild annealing temperatures. This lack of a stable IMC phase suggests that there is no thermodynamic driving force for intermixing of Pd and Ni. We have performed DFT analysis to support this hypothesis, which will be discussed in detail below. Further, our experimental results show that the outer shell remains of a consistent thickness despite annealing, indicating limited diffusion between the core and shell. By intermixing the multilayered shell of defined core-shell structures, we can begin to construct a set of design parameters to be extended to other IMC NP structures of various shapes and compositions.

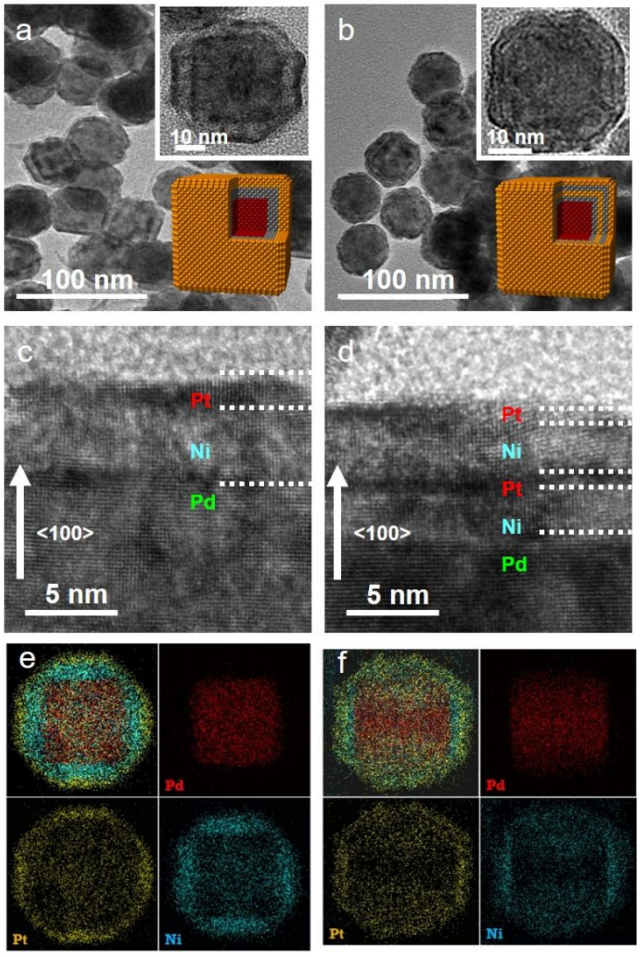

Figure 1: Transmission electron microscopy images of the as-synthesized (a) Pd-Ni-Pt samples at low magnification with the inset showing a single precursor particle and (b) Pd-(Ni-Pt)$_2$ samples at low magnification with the inset showing a single precursor particle. (c and d) show high magnification images of the Pd-Ni-Pt and Pd-(Ni-Pt)$_2$ particles, respectively, with the lighter Ni phase "sandwiched" between the darker Pd and Pt phases. (e and f) Energy dispersive x-ray mapping of the Pd, Ni, and Pt phases showing the Pd core and Ni and Pt surface layers.

Representative transmission electron microscopy (TEM) images of the Pd-Ni-Pt (a and c) and the Pd-(Ni-Pt)$_2$ (b and d) core-multilayered shell NP precursors can be seen in Figure 1. Mapping by energy dispersive x-ray spectroscopy (EDX) clearly shows Pd located in the core cube with Ni and Pt layered in the shell. Each layer shows epitaxial overgrowth, even with the high interfacial energy and strain associated with the metal boundary between the highly mismatched (~10%) lattices of Ni and Pt. This induced strain should contribute to a lower effective diffusion barrier facilitating metal-metal migration, particularly through the open (100) facet (which dominates the surface of our cubic NPs). Calculations for the expected thickness of the metallic layers were performed based on atomic ratios obtained through inductively coupled plasma optical emission spectroscopy (ICP-OES). By scanning electron microscopy (SEM), the base Pd cube is found to be ~30 nm in edge length (Figure S1) and, by TEM, the final layered structure, either two- or four-layered, is ~35 nm in edge length. Lattice constants of 352.4 pm and 392.42 pm were used for Ni and Pt, respectively. For the Pd-Ni-Pt particles, layers of 3.6 nm and 1.4 nm were found respectively for the Ni and Pt (3.52 and 1.43 were measured by TEM). The calculation for the four-layered particles assumed that both shell layers were of equivalent thickness for each metal. Based on this assumption, thicknesses of 1.7 nm and 0.8 nm (1.78 nm and 0.77 nm were measured by TEM) were found for Ni and Pt, respectively. The experimental ratios were found to be Pd-Ni$_{3.1}$-Pt for the two-layered samples and Pd-(Ni$_{1.3}$-Pt$_{0.5}$)$_2$ for the four-layered samples, as can be seen in Table S1. These values are close to target value of 3:1 and the expected values from the nominal concentration loading.

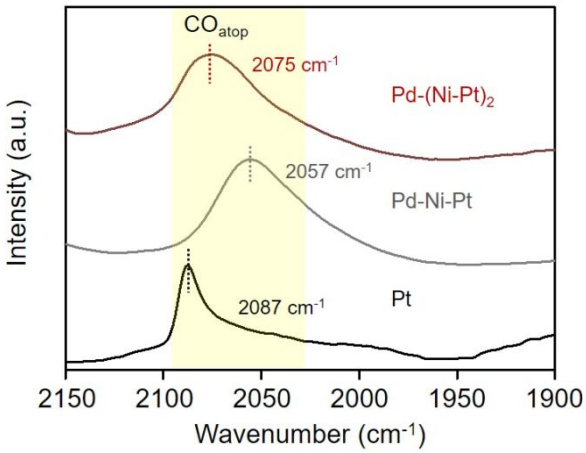

Figure 2: Normalized CO-DRIFTS spectra showing a shift in the energy of the characteristic C-O stretching peak. A larger shift in energy is seen for the thicker-layered Pd-Ni-Pt than the thinner-layered Pd-(Ni-Pt)$_2$.

CO-adsorbed monitored diffusion reflectance infrared spectroscopy (CO-DRIFTS) was used to monitor the initial structure of the NP surface (Figure 2)[44-45]. In each case, the NPs are supported on SiO_2. For pure Pt NPs, a characteristic C-O stretch is seen around 2087 cm^{-1}, corresponding to CO adsorbed on atop Pt [46-47]. When Ni is introduced below the Pt surface in the two-layered structure, a shift in the C-O peak to 2057 cm^{-1} is seen.

This shift could be attributed to the ligand effect. Ni has a Fermi level energy of 9.46 eV while the Fermi level of Pt sits at 8.79 eV[48]. As such, charge is transferred from the inner Ni layer to the outer Pt layer. This filling of the Pt d-band lowers its energy, which changes its interaction with CO and shifts the C-O stretch frequency.[49] By the same logic, we should observe a larger shift for the four-layered samples because the Pt layer is thinner and thus the surface Pt is closer to the Ni layer. However, the band of Pd-(Ni-Pt)$_2$ shifts only 15 cm^{-1} from original Pt. This observation could be attributed to the effect of increased strain in the four-layered system. Compressive strain from Ni serves to shift the Pt d-band higher in energy, offsetting some of the shift induced by the ligand effect. This result suggests that Pd-(Ni-Pt)$_2$ shows increased strain compared with Pd-Ni-Pt.

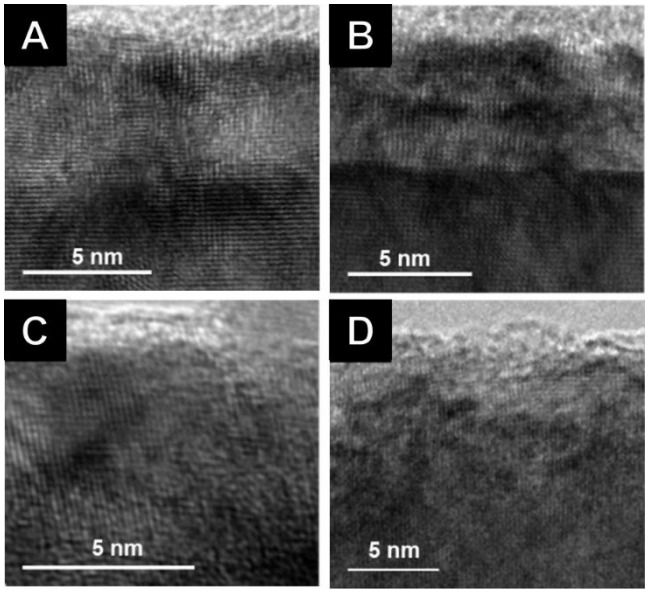

Figure 3: Representative high-resolution TEM images from which the quantitative lattice spacing data are calculated. (a and b) Pd-Ni-Pt and Pd-(Ni-Pt)$_2$, respectively, after annealing at 200 °C. Layering is still visible by contrast in the image. (c and d) Pd-Ni-Pt and Pd-(Ni-Pt)$_2$ after annealing at 400 °C. One mixed layer can be seen for the Pd-(Ni-Pt)$_2$ sample.

To more quantitatively track the degree of mixing for each temperature, high-resolution TEM (HRTEM) images were taken to study the change in lattice parameter through the different layers of the NP. Figure 3 shows representative HRTEM images taken of each sample at three different temperatures in the [200] direction. For pristine Pd, Ni, and Pt, the d-spacing measurements in the [200] direction are 0.1945 nm, 0.1760 nm, 0.1960 nm, respectively. (XRD) With the migration of the metal atoms, the lattice spacing is expected to change due to the different lattice constants. The larger Pt lattice will compress due to epitaxy with and incorporation of Ni while Ni will expand. Once completely mixed and stable, the lattice measurements throughout the mixed shell should be the same (~0.1875 nm). Figure 4 shows a graphical representation of the changes in the lattice parameters from the Pt shell down to the Pd core. At 200 °C a clear difference can be seen between the mixing in the two structures. The four-layered, strained structure shows mixing initiated at the Ni/Pt interfaces, while clear, separated Ni and Pt layers are seen in the two-layered structure. At 300 °C, the four-layered structure begins to approach full mixing and the two-layered shows the beginning of it at the Ni/Pt interface. At 400 °C, the shell of Pd-(Ni-Pt)$_2$ is fully mixed, while Ni and Pt layers are still visible in Pd-Ni-Pt. Overall, this analysis reinforces our idea that increased strain in Pd-(Ni-Pt)$_2$ allows for mixing at lower temperatures.

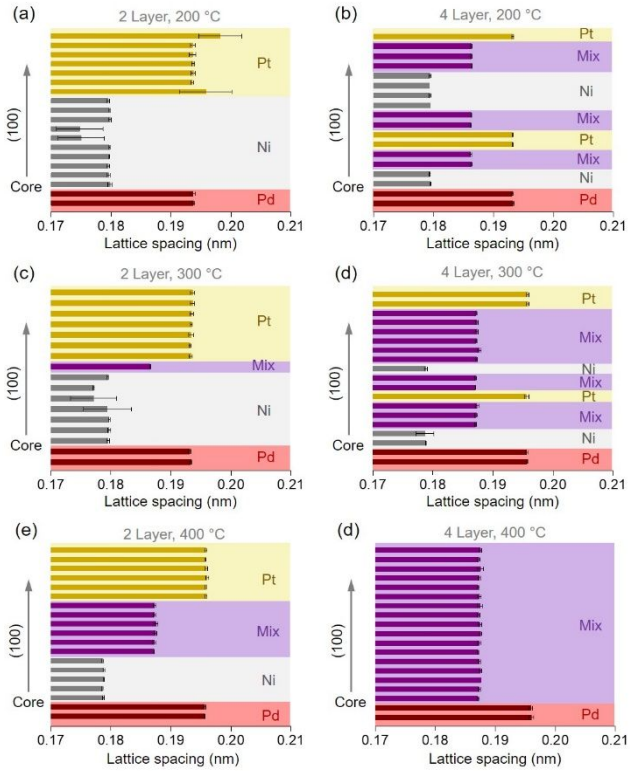

Figure 4. Lattice spacing measurement of Pd (red), Ni (grey), Pt (gold), and intermixed layered (purple). The intermixing is more pronounced at lower annealing temperatures for four-layered samples compared to the two-layered sample.

These quantitative data agree well with our post-annealing characterization by EDX (Figure 5). Mixing can be seen in the outer shell layers after annealing at 400 °C. Importantly, the Pd cube is clearly visible in the core of the mixed particle. This supports our hypothesis that Pd will not migrate into the shell layers at the mild temperatures chosen for our annealing.

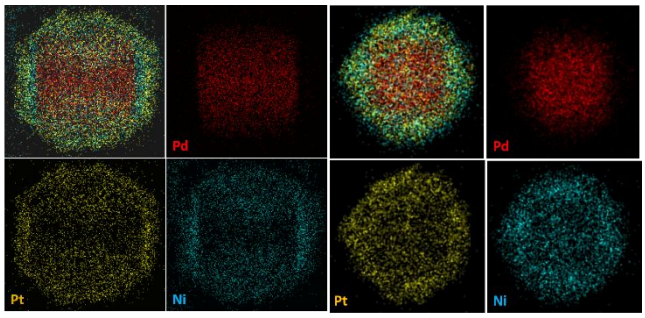

Figure 5. Energy dispersive x-ray images of Pd-(Ni-Pt)$_2$ (left) before and (right) after annealing, showing the core Pd cube and the mixing of the outer layers.

Next, we discuss theoretical insights intoenergetics relevant to this lower-temperature intermixing in this system using Density Functional Theory (DFT) analysis. Additional details and results are provided in the SI. As a preliminary analysis, using the PBEsol functional, the result support our hypothesis that intermixing of Ni and Pt to form Ni_3Pt is thermodynamically favored by 0.27 eV (per 3 Ni + 1 Pt), but intermixing of Ni and Pd to for Ni_3Pd is disfavored by 0.13 eV (per 3 Ni + 1 Pd). We have also checked that intermixing of Ni with Pt is favored, and with Pd is disfavored, for other stoichiometries (Table S2). Regarding the kinetics of intermixing, we first performed a benchmark analysis for the vacancy-mediated diffusion of Ni in bulk Pt. Here, a vacancy diffuses through Pt to a site adjacent to the Ni impurity, thereby allowing Ni to hop to that adjacent site. The effective barrier, E_{eff}, for such a process is the sum of a barrier for an atom hopping into an adjacent vacancy, E_{dv}, and a formation energy for creating the vacancy, E_{fv}[50]. Nuances are described below[51]. Here, we only report results from the PBEsol functional, which has been shown to be reliable for vacancy diffusion[52]. For the diffusion of Ni in Pt, the barrier for the Ni impurity to hop into an adjacent vacancy is found to be E_{dv} = 0.93

eV (versus E_{dv} = 1.4 eV for a Pt atom to hop into an adjacent vacancy in Pt). Thus, diffusion of the vacancy through Pt to reach a site adjacent to the Ni impurity (rather than the hopping of Ni into the vacancy) is the rate-controlling step. Consequently, the higher E_{dv} = 1.4 eV determines E_{eff}. The formation energy for a vacancy next to a Ni impurity in Pt is E_{fv} = 0.94 eV (versus E_{fv} = 0.84 eV for formation of a vacancy in pure Pt), and the former higher value determines E_{eff}. However, DFT underestimates E_{fv} due to so-called "surface intrinsic error", so, guided by previous analysis for pure Pt[50], we use E_{fv} = 1.2 eV (rather than 0.94 eV) to obtain $E_{eff} \approx 1.4 + 1.2 = 2.6$ eV for Ni diffusion in Pt. The corresponding effective rate for hopping of the Ni impurity, assuming an Arrhenius form with a typical prefactor of 10^{13}/s is about $10^{-6.5}$/s at 400 °C, too low for effective intermixing on the experimental timescale.

However, motivated by the proposed importance of strain effects in intermixing, we consider the effect of compressive Pt strain, $\varepsilon < 0$, on E_{fv}, and E_{dv}. (Recall that epitaxy at the Ni-Pt interface within the NP, as well as Ni incorporation into Pt, should induce compressive strain.) Significantly, we find a strong decrease in the vacancy formation energy, E_{fv}, with increasing strain magnitude, $|\varepsilon|$, for triaxial strain, and, in fact, E_{fv} vanishes when $|\varepsilon|$ increases to only 2%. A weaker decrease occurs for biaxial strain. On the other hand, E_{dv} increases with $|\varepsilon|$ to 1.2 eV (1.7 eV) for Ni (Pt) hopping into a vacancy where $|\varepsilon|$ = 2% for triaxial strain (with a lesser increase for biaxial strain). Assuming that compressive strain makes E_{fv} negligible, then $E_{eff} \approx E_{dv} \approx 1.6$ eV. Then, the effective hop rate for the Ni impurity is about 10/s, which is sufficiently high for effective intermixing.

Second, we briefly consider the vacancy-mediated diffusion of Pt in bulk Ni. PBEsol predicts that E_{dv} = 1.4 eV (1.2 eV) for a Pt (Ni) atom to hop into an adjacent vacancy in Ni. PBEsol also predicts that E_{fv} = 1.5 eV for vacancy formation next to a Pt impurity in Ni and E_{fv} = 1.6 eV in pure Ni (which might be increased by ~0.2 eV accounting for surface intrinsic error). Thus, we conclude that $E_{eff} \approx 1.4 + 1.8 = 3.2$ eV, too high for this intermixing process to be effective. Additional studies to explore the effect of tensile strain on Ni (induced by epitaxy at the Ni-Pt interfaces and Pt incorporation in Ni) reveal that E_{fv} actually increases with strain (at least up to ~6%). Although E_{dv} increases somewhat, there is no net decrease in E_{eff}. Thus, we conclude that intermixing in the Ni-Pt system is asymmetric and associated with strain-enhanced diffusion of Ni into Pt, rather than by Pt diffusion into Ni, which is in agreement with previous experimental results[53].

To further investigate surface structure, each sample was tested for the alkaline methanol electro-oxidation reaction (MOR), a typical small molecule oxidation reaction with potential in fuel cell applications. Electrochemical measurements illuminate the surface electronic structure of the catalyst by testing its ability to perform desired transformations. Pt-Ni composites have been shown to display high MOR activity, as charge transfer brings the metal d-band to an optimal energy level[54]. The performance and durability of MOR catalysts can be negatively impacted by the (often irreversible) adsorption of a CO intermediate, but it has been shown that intermetallic structures are less prone to CO poisoning[55]. They are also more resistant to etching in acidic media, showcasing higher stability as a result. Each sample was loaded on Vulcan XC-72 carbon and dried under nitrogen for 24 hours. The

electrochemical conversions were performed using a standard three-electrode system: Pt wire as the counter electrode, saturated calomel electrode as the reference electrode, and a glassy carbon electrode loaded with 5 μL of the synthesized nanocatalysts supported on Vulcan carbon as the working electrode.

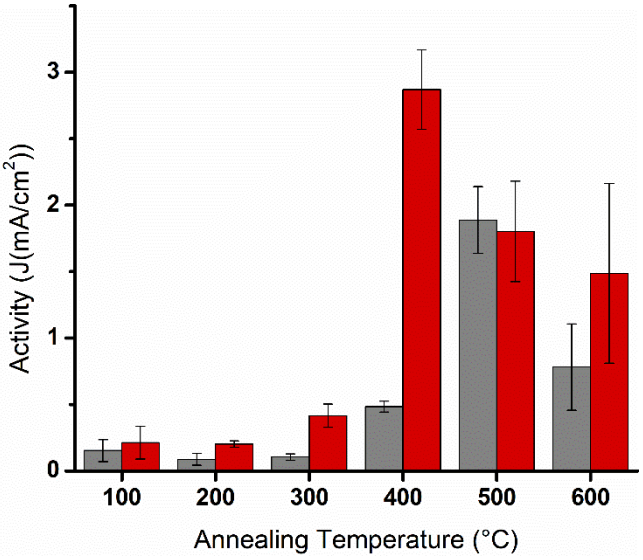

Figure 6. Electrochemical activity for methanol oxidation catalyzed by Pd-Ni-Pt and Pd-(Ni-Pt)$_2$ NPs annealed at various temperatures. Grey bars represent the two-layered Pd-Ni-Pt and red bars represent the four-layered Pd-(Ni-Pt)$_2$.

From Figure 6, a comparison of each sample (two- and four-layered) at the designated temperatures can be seen. At 200 °C, both samples perform nominally the same as the as-synthesized samples. At 300 °C, each sample has a slight increase in activity, but the four-layered sample, with its higher lattice strain and thus greater degree of mixing, does see a somewhat larger increase. By 400 °C, as strain allows complete mixing throughout the multilayered shell, the four-layered sample has a significant jump in activity. This complete mixing can be seen in the lattice spacing measurements (Figure 4), and the mixed shell yields a more active surface. However, at the same temperature, the two-layered sample has only a minor increase in activity, on par with the four-layered sample at 300 °C, as it is only partially mixed, which we attribute to the lesser strain in its thicker layers. We moved to higher temperatures to see if we could induce the same degree of migration in the two-layered sample as seen in the four-layered. By 500 °C, a larger jump in activity is observed. The four-layered sample, meanwhile, decreases in activity. This deactivation of the four-layered catalyst is attributed to the degradation of the sample (i.e. NP sintering) at such high annealing temperatures. To test whether the two-layered structure would follow suit at higher temperatures, an annealing temperature of 600 °C was used; the same dip in activity was observed. Each sample and temperature profile was run in triplicate, leading to the errors bars depicted. We again attribute the large error bars at high temperatures to sample degradation at these high temperatures, which is not a reproducible process. Moreover, the change in the surface structure also causes breaks in the consistency of the active sites, which would also lead to a higher degree of error.

The temperatures chosen for IMC synthesis beg two questions: First, is the annealing time of one-hour ideal for the mixing process? Perhaps a longer annealing time at a lower temperature could prevent aggregation and preserve fidelity to the initial cubic NP shape. Second, can the Pd-Ni-Pt NPs achieve an activity comparable to the Pd-(Ni-Pt)$_2$ NPs if given more time to mix? These questions were addressed using extended time studies, annealing the NPs for longer times at each temperature, as shown in Figure S6.

Annealing for longer than one hour at 200 °C appears to have little effect on the catalytic activity, for both the Pd-Ni-Pt and Pd-(Ni-Pt)$_2$ NPs, implying that the low annealing temperature is unable to overcome the kinetic barriers associated with mixing, irrespective of the annealing time. This experiment agrees well with our DFT results and supports the need to increase annealing temperatures in order to induce metallic mixing. The extended annealing at 400 °C shows two distinct effects for the Pd-Ni-Pt and Pd-(Ni-Pt)$_2$ NPs. For Pd-(Ni-Pt)$_2$, extending the annealing time to two hours led to no change in activity, so further studies were not carried out. This result makes sense, as the outer shell is already fully mixed after 1 h. For Pd-Ni-Pt, activity continues to increase up to a five-hour annealing time. This result suggests that, given enough time, the thicker Ni and Pt layers can achieve mixing similar to the thinner layers in Pd-(Ni-Pt)$_2$. After more than five hours, the activity decreases, which we attribute to surface roughening and sintering after such a long annealing process at high temperature.

In conclusion, we have used a variety of techniques to investigate metallic mixing on the nanoscale. Through TEM and HRTEM analysis, we have shown that atomic diffusion is dependent on the thickness of the layers that make up the mixing metals. Through CO-DRIFTS, we have shown that our shell layers increase strain on the outer Pt surface, which DFT calculations suggest is essential for low-temperature metallic mixing. Through MOR, we have shown that this mixing changes the electronic structure of the active metal surface, with clear differences again seen between the layered Pd-Ni-Pt and Pd-(Ni-Pt)$_2$ nanostructures. Overall, the insight gained represents an important step toward the development of shape-controlled bimetallic and IMC NPs. In the future, our platform can be extended to more exotic crystal structures beyond the *fcc*, d-block metals presented here, with an eye toward the ultimate goal of generating a set of design rules for the synthesis of nanocatalysts with custom-made geometric and electronic surface structure.

ACKNOWLEDGMENT

B.P.W. and C.-K.T. were partially supported by NSF Grant CHE-1566445. Y.H was supported for the DFT analysis by NSF Grant CHE-1507223, and acknowledges use of XSEDE resources operated under NSF grant ACI-1548562. J.W.E was supported for the theoretical analysis by the US Department of Energy, Office of Science, Basic Energy Sciences, Division of Chemical, Sciences, Geosciences, and Biological Sciences, and his work was performed at Ames Laboratory which is operated by Iowa State University under contract No. DE-AC02-07CH11338. Use of resources from NERSC, a USDOE Office of Science User Facility operated under contract No. DE-AC02-05CH11231, is also acknowledged.

REFERENCE

1. Li, L. D.; Zhou, L.; Ould-Chikh, S.; Anjum, D. H.; Kanoun, M. B.; Scaranto, J.; Hedhili, M. N.; Khalid, S.; Laveille, P. V.; D'Souza, L.; Clo, A.; Basset, J. M., Controlled Surface Segregation Leads to Efficient Coke-Resistant Nickel/Platinum Bimetallic Catalysts for the Dry Reforming of Methane. *Chemcatchem* **2015,** *7* (5), 819-829.
2. Li, X.; An, L.; Chen, X.; Zhang, N. L.; Xia, D. G.; Huang, W. F.; Chu, W. S.; Wu, Z. Y., Durability Enhancement of Intermetallics Electrocatalysts via N-anchor Effect for Fuel Cells. *Sci Rep-Uk* **2013,** *3*.
3. Xia, T. Y.; Liu, J. L.; Wang, S. G.; Wang, C.; Sun, Y.; Gu, L.; Wang, R. M., Enhanced Catalytic Activities of NiPt Truncated Octahedral Nanoparticles toward Ethylene

Glycol Oxidation and Oxygen Reduction in Alkaline Electrolyte. *Acs Appl Mater Inter* **2016,** *8* (17), 10841-10849.
4. Xu, S. C.; Walter, E. D.; Zhao, Z. C.; Hu, M. Y.; Han, X. W.; Hu, J. Z.; Bao, X. H., Dynamic Structural Changes of SiO2 Supported Pt-Ni Bimetallic Catalysts over Redox Treatments Revealed by NMR and EPR. *J Phys Chem C* **2015,** *119* (36), 21219-21226.
5. Zhu, Z. J.; Zhai, Y. L.; Dong, S. J., Facial Synthesis of PtM (M = Fe, Co, Cu, Ni) Bimetallic Alloy Nanosponges and Their Enhanced Catalysis for Oxygen Reduction Reaction. *Acs Appl Mater Inter* **2014,** *6* (19), 16721-16726.
6. Zhang, S.; Zhang, X.; Jiang, G. M.; Zhu, H. Y.; Guo, S. J.; Su, D.; Lu, G.; Sun, S. H., Tuning Nanoparticle Structure and Surface Strain for Catalysis Optimization. *J Am Chem Soc* **2014,** *136* (21), 7734-7739.
7. Zhu, J.; Yang, Y.; Chen, L.; Xiao, W.; Liu, H.; Abruna, H. D.; Wang, D., Copper-Induced Formation of Structurally Ordered Pt-Fe-Cu Ternary Intermetallic Electrocatalysts with Tunable Phase Structure and Improved Stability. *Chemistry of Materials* **2018,** *30*, 5987-5995.
8. Bhunia, K.; Khilari, S.; Pradhan, D., Monodispersed PtPdNi Trimetallic Nanoparticles-Integrated Reduced Graphene Oxide Hybrid Platform for Direct Alcohol Fuel Cell. *ACS Sustainable Chemistry & Engineering* **2018,** *6* (6), 7769-7778.
9. Ross, M. B.; De Luna, P.; Li, Y.; Dinh, C.-T.; Kim, D.; Yang, P.; Sargent, E. H., Designing materials for electrochemcial carbon dioxide recycling. *Nature Catalysis* **2019**, Ahead of Print.
10. Zou, L. F., J; Zhou, Y; Wang, C; Li, J; Zou, Z; Yang, H, Conversion of PtNi alloy from disordered to ordered for enhanced activity and durability of methanol tolerant oxygen reduction reaction. *Nano Research* **2015,** *8* (8), 2777-2788.
11. Cui, C. G., L; Li, H; Yu, S; Heggen, M; Strasser, P, Octahedral PtNi Nanoparticle Catalysts: Exceptional Oxygen Reduction Activity by Tuning the Alloy Particle Surface Composition. *Nano Letters* **2012,** *12*, 5885-5889.
12. Sneed, B. B., C; Kuo, C.H; Lamontagne, L; Jiang, Y; Wang, Y; Tao, F; Huang, W; Tsung, C.K, Nanoscale-Phase-Separated Pd-Rh Boxes Synthesized via Metal Migration: An Archetype for Studying Lattice Strain and Composition Effects in Electrocatalysis. *J Am Chem Soc* **2013,** *135* (39), 14691-14700.
13. Sneed, B. Y., A; Jalalpoor, D; Golden, M; Mao, S; Jiang, Y; Wang, Y; Tsung C.K, Shaped Pd-Ni-Pt Core-Sandwich-Shell Nanoparticles: Influence of Ni Sandwich Layers on Catalytic Electrooxidations. *ACS Nano* **2014,** *8* (7), 7239-7250.
14. Park, K. W. C., J.H; Kwon, B.K; Lee, S.A; Sung, Y.E, Chemical and Electronic Effects of Ni in Pt/Ni and Pt/Ru/Ni Alloy Nanoparticles in Methanol Electrooxidation. *The Journal of Physical Chemistry B* **2002,** *106* (8), 1869-1877.
15. Yang, H. V., W; Lamy, C; Alonso-Vante, N, Structure and Electrocatalytic Activity of Carbon-Supported Pt-Ni Alloy Nanoparticles Toward the Oxygen Reduction Reaction. *The Journal of Physical Chemistry B* **2004,** *108* (30), 11024-11034.
16. Strasser, P.; Kuehl, S., Dealloyed Pt-based core-shell oxygen reduction electrocatalysts. *Nano Energy* **2016,** *29*, 166-177.
17. Gamler, J. T.; Ashberry, H. M.; Skrabalak, S. E.; Koczkur, K. M., Random Alloyed versus Intermetallic Nanoparticles: A Comparison of Electrocatalytic Performance. *Advanced Materials* **2018,** *30* (40), 1801563.
18. Wolff, I. M.; Hill, P. J., Platinum Metals-Based Intermetallics for High-Temperature Service. *Platin Met Rev* **2000,** *44* (4), 158-166.
19. Hasché, F. O., M; Strasser, P, Activity, Structure and Degradation of Dealloyed PtNi3 Nanoparticle Electrocatalyst for the Oxygen Reduction Reaction in PEMFC. *Journal of the Electrochemical Society* **2012,** *159* (1), B24-B33.
20. Dikshtein, I.; Koledov, V.; Shavrov, V.; Tulaikova, A.; Cherechukin, A.; Buchelnikov, V.; Khovailo, V.; Matsumoto, M.; Takagi, T.; Tani, J., Phase transitions in intermetallic compounds Ni-Mn-Ga with shape memory effect. *IEEE Transactions on Magnetics* **1999,** *35* (5), 3811-3813.
21. Evans, M. J.; Wu, Y.; Kranak, V. F.; Newman, N.; Reller, A.; Garcia-Garcia, F. J.; Haeussermann, U., Structural properties and superconductivity in the ternary intermetallic compounds MAB (M=Ca, Sr, Ba; A=Al, Ga, In; B=Si, Ge, Sn). *Physical Review B* **2009,** *80* (6), 064514.
22. Fernandez, J. F.; Cuevas, F.; Leardini, F.; Bodega, J.; Ares, J. R.; Garces, G.; Perez, P.; Sanchez, C., A new pseudo-binary Mg(6)Ni(0.5)Pd(0.5) intermetallic compound stabilised by Pd for hydrogen storage. *Journal of Alloys and Compounds* **2010,** *495* (2), 663-666.
23. Zhao, Y.; Yu, J. K.; Wu, L. L.; Wan, B.; Zhang, Y. K.; Gao, R.; Zhang, J. W.; Gou, H. Y., Mechanical properties and electronic structures of diverse Pt-Al intermetallics: First-principles calculations. *Comp Mater Sci* **2016,** *124*, 273-281.
24. Furukawa, S.; Ehara, K.; Ozawa, K.; Komatsu, T., A study on the hydrogen activation properties of Ni-based intermetallics: a relationship between reactivity and the electronic state. *Phys Chem Chem Phys* **2014,** *16* (37), 19828-19831.
25. Xiao, W.; Lei, W.; Gong, M.; Xin, H. L.; Wang, D., Recent Advances of Structurally Ordered Intermetallic Nanoparticles for Electrocatalysis. *ACS Catalysis* **2018,** *8* (4), 3237-3256.

26. Besenbacher, F.; Chorkendorff, I.; Clausen, B. S.; Hammer, B.; Molenbroek, A. M.; Norskov, J. K.; Stensgaard, I., Design of a surface alloy catalyst for steam reforming. *Science* **1998,** *279* (5358), 1913-1915.
27. Studt, F.; Abild-Pedersen, F.; Bligaard, T.; Sorensen, R. Z.; Christensen, C. H.; Norskov, J. K., Identification of non-precious metal alloy catalysts for selective hydrogenation of acetylene. *Science* **2008,** *320* (5881), 1320-1322.
28. Armbruster, M.; Kovnir, K.; Friedrich, M.; Teschner, D.; Wowsnick, G.; Hahne, M.; Gille, P.; Szentmiklósi, L.; Feuerbacher, M.; Heggen, M.; Girgsdies, F.; Rosenthal, D.; Schlogl, R.; Grin, Y., Al13Fe4 as a low-cost alternative for palladium in heterogeneous hydrogenation. *Nature Materials* **2012,** *11* (8), 690-693.
29. Yan, Y.; Du, J. S.; Gilroy, K. D.; Yang, D.; Xia, Y.; Zhang, H., Intermetallic Nanocrystals: Syntheses and Catalytic Applications. *Advanced Materials* **2017,** *29* (14), 1605997.
30. Feng, Q.; Zhao, S.; Wang, Y.; Dong, J.; Chen, W.; He, D.; Wang, D.; Yang, J.; Zhu, Y.; Zhu, H.; Gu, L.; Li, Z.; Liu, Y.; Yu, R.; Li, J.; Li, Y., Isolated Single-Atom Pd Sites in Intermetallic Nanostructures: High Catalytic Selectivity for Semihydrogenation of Alkynes. *J Am Chem Soc* **2017,** *139* (21), 7294-7301.
31. Furukawa, S.; Komatsu, T., Intermetallic Compounds: Promising Inorganic Materials for Well-Structured and Electronically Modified Reaction Environments for Efficient Catalysis. *ACS Catalysis* **2017,** *7* (1), 735-765.
32. Zhou, H.; Yang, X.; Li, L.; Liu, X.; Huang, Y.; Pan, X.; Wang, A.; Li, J.; Zhang, T., PdZn Intermetallic Nanostructure with Pd-Zn-Pd Ensembles for Highly Active and Chemoselective Semi-Hydrogenation of Acetylene. *ACS Catalysis* **2016,** *6* (2), 1054-1061.
33. Maligal-Ganesh, R.; Xiao, C.; Goh, T. W.; Wang, L.-L.; Gustafson, J.; Pei, Y.; Qi, Z.; Johnson, D. D.; Zhang, S.; Tao, F.; Huang, W., A Ship-in-a-Bottle Strategy to Synthesize Encapsulated Intermetallic Nanoparticle Catalysts: Exemplified for Furfural Hydrogenation. *ACS Catalysis* **2016,** *6* (3), 1754-1763.
34. Enayati, M. H.; Salehi, M., Formation mechanism of Fe_3Al and FeAl intermetallic compounds during mechanical alloying. *J. Mater. Sci.* **2005,** *40*, 3933-3938.
35. Furukawa, S.; Komatsu, T., Intermetallic Compounds: Promising Inorganic Materials for Well-Structured and Electronically Modified Reaction Environments for Efficient Catalysis. *ACS Catalysis* **2017,** (7), 735-765.
36. Schaefer, Z. L.; Vaughn II, D. D.; Schaak, R. E., Solution chemistry synthesis, morphology studies, and optical properties of distinct nanocrystalline Au-Zn intermetallic compounds. *J. Alloy Compd.* **2010,** *490*, 98-102.
37. Maksimuk, S.; Yang, S.; Peng, Z.; Yang, H., Synthesis and Characterization of Ordered Intermetallic PtPb Nanorods. *J. Am. Chem. Soc.* **2007,** *129*, 8684-8685.
38. Leonard, B. M.; Zhou, Q.; Wu, D.; DiSalvo, F. J., Facile Synthesis of PtNi Intermetallic Nanoparticles: Influence of Reducing Agent and Precursors on Electrocatalytic Activity. *Chem. Mater.* **2011,** (23), 1136-1146.
39. Wang, D. S.; Peng, Q.; Li, Y. D., Nanocrystalline Intermetallics and Alloys. *Nano Research* **2010,** *3* (8), 574-580.
40. Belova, I. V.; Murch, G. E., Interdiffusion in Intermetallics. *Metall Mater Trans A* **2013,** *44A* (10), 4417-4421.
41. Mehrer, H., Diffusion in intermetallics. *Mater T Jim* **1996,** *37* (6), 1259-1280.
42. Brodsky, C. Y., A; Ng, K; Kuo, C.H.; Tsung, C.K., Electrochemically Induced Surface Metal Migration in Well-Defined Core-Shell Nanoparticles and Its General Influence on Electrocatalytic Reactions. *ACS Nano* **2014,** *8* (9), 9368-9378.
43. Leonard, B. Z., Q; Wu, D; DiSalvo, F, Facile Synthesis of PtNi Intermetallic Nanoparticles: Influence of Reducing Agent and Precursors on Electrocatalytic Activity. *Chemistry of Materials* **2011,** *23*, 1136-1146.
44. Vimont, A.; Thibault-Starzyk, F.; Daturi, M., Analysing and understanding the active site by IR spectroscopy. *Chem. Soc. Rev.* **2010,** *39* (12), 4928-4950.
45. Unterhalt, H.; Rupprechter, G.; Freund, H.-J., Vibrational Sum Frequency Spectroscopy on Pd(111) and Supported Pd Nanoparticles: CO Adsorption from Ultrahigh Vacuum to Atmospheric Pressure. *J. Phys. Chem. B* **2002,** *106* (2), 356-367.
46. Crossley, A.; King, D. A., Infrared spectra for co isotopes chemisorbed on Pt "111": Evidence for strong absorbate coupling interactions. *Surf. Sci.* **1977,** *68*, 528-538.
47. Primet, M., Electronic transfer and ligand effects in the infrared spectra of adsorbed carbon monoxide. *Journal of Catalysis* **1984,** *88* (2), 273-282.
48. Sigalas, M.; Papaconstantopoulos, D. A.; Bacalis, N. C., Total energy and band structure of the 3d, 4d, and 5d metals. *Physical Review B* **1991,** *45*, 5777-5783.
49. Pei, Y.; Qi, Z.; Goh, T. W.; Wang, L.-L.; Maligal-Ganesh, R. V.; MacMurdo, H. L.; Zhang, S.; Xiao, C.; Li, X.; Tao, F. F.; Johnson, D. D.; huang, W., Intermetallic structures with atomic precision for selective hydrogenation of nitroarenes. *Journal of Catalysis* **2017,** *356*, 307-314.
50. Mattsson, T. R.; Mattsson, A. E., Calculating the vacancy formation energy in metals: Pt, Pd, and Mo. *Physical Review B* **2002,** *66*, 214110.
51. Lai, K. C.; Han, Y.; Spurgeon, P.; Huang, W.; Thiel, P. A.; Liu, D.-J.; Evans, J. W., Reshaping,

intermixing, and coarsening for metallic nanocrystals: Non-equilibrium statistical mechanical and coarse-grained modeling. *Chemical Reviews* **2019,** *119*, 6670-6678.
52. Chen, M.; Han, Y.; Goh, T. W.; Sun, R.; Maligal-Ganesh, R. V.; Pei, Y.; Tsung, C.-K.; Evans, J. W.; Huang, W., Kinetics, Energetics, and Size-dependence of the Transformation from Pt to Ordered PtSn Intermetallic Nanoparticles. *Nanoscale* **2019,** *11*, 5336-5345.
53. Chen, C.; Kang, Y.; Huo, Z.; Zhu, Z.; Huang, W.; Xin, H. L.; Snyder, J. D.; Li, D.; Herron, J. A.; Mavrikakis, M.; Chi, M.; More, K. L.; Li, Y.; Markovic, N. M.; Somorjai, G. A.; Yang, P.; Stamenkovic, V. R., Highly Crystalline Multimetallic Nanoframes with Three-Dimensional Electrocatalytic Surfaces. *Science* **2014,** *343*, 1339-1343.
54. Liu, X.-J.; Cui, C.-H.; Gong, M.; Li, H.-H.; Xue, Y.; Fan, F.-J.; Yu, S.-H., Pt-Ni alloyed nanocrystals with controlled architectures for enhanced methanol oxidation. *Chemical Communications* **2013,** *49*, 8704-8706.
55. Qi, Z.; Xiao, C.; Liu, C.; Goh, T. W.; Zhou, L.; Maligal-Ganesh, R.; Pei, Y.; Li, X.; Curtiss, L. A.; Huang, W., Sub-4 nm PtZn Intermetallic Nanoparticles for Enhanced Mass and Specific Activities in Catalytic Electrooxidation Reaction. *Journal of the American Chemical Society* **2017,** *139* (13), 4762-4768.